Enhanced magnetic moments in bcc Fe films

J. A. C. Bland and C. Daboo
Cavendish Laboratory, Madingley Road, Cambridge CB3 0HE, United Kingdom

B. Heinrich and Z. Celinski*
Physics Department, Simon Fraser University, Burnaby, British Columbia, Canada V5A 1S6

R. D. Bateson
European Synchrotron Radiation Facility, Boîte Postale 220, F38043, Grenoble Cedex, France
(Received 14 April 1994; revised manuscript received 19 July 1994)

We present evidence for enhanced magnetic moments in epitaxial Fe films in proximity with Ag, Au, Cu, and Pd overlayers prepared by molecular-beam epitaxy on singular Ag(001) substrates in a combined study using polarized-neutron reflection (PNR) and ferromagnetic resonance (FMR). Second versions of equivalent samples were investigated in order to test the repeatability of the results, and all PNR measurements were corrected for background and diffuse scattering. Within experimental error, measurements of the absolute value of the magnetic moment per atom made using PNR were found to agree with measurements of the relative magnetization using FMR, and measurements on repeated samples were also found to agree. An average magnetic moment per Fe atom of $2.58\pm0.09\mu_B$ was determined for a Ag/5.5 ML Fe structure, significantly enhanced from the value of $\mu_{Fe}=2.33\pm0.05\mu_B$ obtained for a Ag/10.9 ML Fe reference sample. Corresponding values of $2.48\pm0.08\mu_B$ and $2.50\pm0.10\mu_B$ were determined for Cu/5.8 ML Fe and Cu/5.7 ML Fe structures, respectively. Values of the layer averaged moment of $2.66\pm0.05\mu_B$ and $2.6\pm0.2\mu_B$ were determined for Pd/5.6 ML Fe and Pd/5.7 ML Fe structures, respectively, assuming that no induced polarization occurs in the interface Pd layers. The degree of enhancement measured in equivalent samples is seen to be in agreement within experimental error. The magnitude of the enhancement (12–20)% we observe in the samples of thickness close to 6 ML is slightly higher than that predicted by recent band-structure calculations, but our results show conclusively that the enhancement can be attributed to the interface atoms. The temperature dependence of the magnetization has also been measured using PNR and the results compared with that predicted from spin-wave theory using FMR measurements of the effective spin-wave gap. Good agreement is found for the Ag/Fe and Cu/Fe systems for which spin-wave gap temperatures of 0.1 and 0.12 K, respectively, are determined by PNR, compared with values of 0.15 and 0.11 K deduced from FMR, where the agreement for Au/Fe is less good. Both FMR and PNR data are consistent with the largest gap occurring for the Pd/Fe interface system but the value of the spin-wave gap determined by FMR is in this case smaller than the value obtained from fitting the PNR data.

I. INTRODUCTION

The pioneering first-principles spin-density functional calculations of Fu, Freeman, and Oguchi[1] predicted substantially enhanced ground-state magnetic moments in transition-metal monolayers of Fe,Cr,Mn, and stimulated experimental studies designed to test these predictions.[2–5] The origin of the enhancement is in part associated with the significantly increased density of $3d$ states, which is only weakly reduced by sp-d hybridization with the noble-metal substrate in the case of Ag or Au, for example. The existence of spin-polarized surface and interface states also plays an important role in determining the resulting magnetic moment in these systems.[6] Many experimental studies have focused on Fe because of its large bulk phase moment ($2.2\mu_B$) and because it can be grown epitaxially on a range of nonmagnetic substrates. For Fe monolayers supported by noble metal (Refs. 7–9), Cu (Ref. 10), and Pd (Ref. 7) substrates, a moment per Fe atom in the range ($2.7-3.2$) μ_B is predicted, with the smallest moments predicted for Fe layers sandwiched by Cu for which large hybridization effects are expected. Pd is of particular interest, since a significant magnetic polarization is thought to be induced by Fe on the Pd interface layers.[7]

While some of the theoretical predictions have been indirectly confirmed by experiments such as photoemission[4] and Mössbauer studies of the hyperfine fields,[2] at present very few direct magnetometric studies[3,5] have been carried out on films supported by noble metals with sufficient accuracy to yield absolute values of the magnetic moment per atom and that distinguish between the degree of enhancement obtained for different overlayer materials. This is due to the several difficulties that need to be overcome in such experiments. First, a precise knowledge of the film thickness, growth mode, strain, and structure is required. The accuracy with which the moment per atom can be determined depends directly upon the accuracy with which the film thickness is known, and the film thickness has to be determined to

0163-1829/95/51(1)/258(15)/$06.00

within a few percent. In many cases the presence of islands and defects in the films in the monolayer range makes magnetometry measurements impossible, the Fe/W(110) system being a possible exception.[3] Many studies have therefore concentrated on the relative thickness dependence of the magnetization. The extreme sensitivity of the magnetic properties of ultrathin magnetic films to growth conditions and structure has also led to a number of conflicting results appearing in the literature. Second, a sufficiently sensitive magnetometric technique is required, in which no substrate signal requiring correction occurs. Superconducting quantum interference device magnetometry, while widely used and offering the advantage of very high sensitivity, suffers from the disadvantage that the magnetic signal, which arises from a diamagnetic substrate such as Ag or Cu, is often comparable with that of the magnetic layer, thus making an absolute measurement extremely difficult and requiring *in situ* measurements during growth. Third, a stronger temperature dependence of the magnetization occurs in ultrathin films in comparison with the bulk. The magnetization at room temperature can be significantly reduced from the ground-state value due to thermally excited spin waves. It is therefore necessary to carry out the magnetization measurement at liquid-helium temperatures, a requirement that frequently conflicts with *in situ* studies.

The aim of the present work is to systematically investigate the magnetic moment per atom in ultrathin Fe/Ag(001) structures using both polarized neutron reflection (PNR) and ferromagnetic resonance (FMR) techniques, extending our previous studies.[11–13] The Fe films were covered with epitaxial overlayers of Au, Ag, Pd, and Cu in order to study the effect of the overlayer on the magnetic moment, and equivalent samples were reproduced to assess the significance of the results. The Fe/Ag(001) epitaxial system is chosen, since the growth of bcc Fe on Ag(001) has been well characterized in previous studies.[14] For Fe films of a few monolayers thickness, reflection high-energy electron diffraction (RHEED) oscillations can be used to determine the layer thickness, and fcc Au, fcc Ag, bcc Cu, and fcc Pd can be stabilized on Fe(001). Absolute moment measurements were carried out using PNR,[15] since it is now well established that the moment per atom can be determined in embedded ultrathin films with an accuracy largely determined by the thickness calibration, and, in particular, no magnetic signal due to the substrate arises. An important requirement of the PNR technique is that the substrate is sufficiently flat, and, in the present work, singular substrates are used. Early PNR studies of the Fe/Ag system were hampered by the effects of roughness scattering associated with the substrate, and conflicting results were obtained.[15,16] In the case of Fe films prepared on vicinal substrates with large roughness, a reduced moment was deduced,[16] suggesting that optically flat substrates are needed to reduce the diffuse scattering contribution in PNR. Subsequent PNR experiments on samples prepared on singular substrates yielded enhanced moments.[12] The effect of diffuse scattering was not included in estimating the value of the magnetic moment per atom, thus limiting the accuracy of this study.

In the present work, the effects of roughness are included in fitting the PNR data using a recently developed model of the diffuse scattering, appropriate for the realistic case of correlated roughness.[13] The effect of roughness is usually modeled using an effective Debye-Waller correction factor for the specular reflectivity, as is often appropriate in x-ray-reflectivity studies. Such a model is strictly appropriate, however, for random roughness. We demonstrate that where significant diffuse scattering occurs, it is essential that the effect of the diffuse scattering is also included in fitting the PNR data, and that diffuse and specular contributions to the detected intensity must be separated. The present work resolves the conflicting results of previous PNR studies[12,16] by demonstrating that the angular acceptance of the detector, in addition to the roughness of the sample, determines the amount of diffuse scattering present in the reflected intensity. As a check on the reliability of the present results, we compared the results of the PNR measurements with the results of FMR studies, which can be used to provide accurate estimates of the relative magnetization with respect to a reference sample. By combining our results, we find conclusive evidence for enhanced moments in the Ag/Fe, Au/Fe, Pd/Fe, and Cu/Fe overlayer systems. The measured temperature dependence of the magnetization is compared with the predictions of the spin-wave model using values of the spin-wave gap determined from FMR measurements of the magnetic anisotropies.

We first describe the samples prepared for the present investigation before summarizing the use of PNR as a magnetometric technique. This is followed by a description of both random and correlated roughness scattering effects in PNR and of the correction of diffuse scattering effects. The results of the magnetic-moment and temperature-dependent measurements are discussed in the final sections of the paper. A description of the FMR measurement technique is given elsewhere.[17]

II. GROWTH OF bcc Fe FILMS

The epitaxial growth of bcc Fe(001) layers on Ag(001) has been described by Heinrich and co-workers.[18–20] Fe grows in the 45°-rotated bcc phase on Ag(001) substrates with the in-plane lattice parameter of the Fe expanded by 0.8% to match the Ag lattice parameter, and fcc-phase Ag and Au overlayers can be stabilized on such Fe(001) epitaxial layers. Ultrathin epitaxial Pd(001) layers grow in a metastable cubic phase on Fe(001) with the in-plane lattice constant expanded by 5.1%,[21] closely corresponding to the critical value at which the onset of ferromagnetism occurs according to the nonrelativistic calculations of Chen, Brener, and Callaway.[22] The vertical lattice contraction is contracted by ~7%, satisfying Poission's ratio.[23] The vertical contraction may explain the absence of ferromagnetism observed in Pd/Fe(001). The epitaxial growth of metastable bcc Cu(001) on Fe(001) occurs with the in-plane Cu lattice parameter 1.2% smaller than that of the Fe substrate.

In the present study, the sandwich structures listed in Table I containing Fe films of 5–5.8 ML thickness in

TABLE I. A summary of the experimental parameters and of the fitted roughness parameters used in determining the moments of each samples described in the text. The samples are grouped into two according to the detector solid angle $\Delta\Omega$ and beam polarization P used for the measurements. The parameters $\Delta q_{\text{eff}}/q_c$, $\sigma^{1/2}$ and w correspond to the effective wave-vector resolution, roughness amplitude, and coherence length estimated from the data (see text).

Sample (Thicknesses in ML)	$\Delta\Omega$ (sterad)	P (%)	$\Delta q_{\text{eff}}/q_c$	$\sigma^{1/2}$ (Å)	w (Å)
20 Au/7 Ag/10.9 Fe/Ag(001)	7×10^{-6}	87	<0.2	12–19	180–220
20 Au/7 Ag/5.5 Fe/Ag(001)					
20 Au/7 Cu/5.8 Fe/Ag(001)					
20 Au/7 Pd/5.6 Fe/Ag(001)					
52 Au/5.7 Fe/Ag(001)	$2-2.8\times10^{-5}$	84	0.2–0.3	12–20	180–220
42 Au/8 Cu/5.7 Fe/Ag(001)					
42 Au/8 Pd/5.7 Fe/Ag(001)					
24 Au/3 Ni/5 Fe/Ag(001)					
20 Au/9 Fe/Ag(001)					

proximity with overlayers of Ag, Au, Cu, and Pd were grown under the same conditions on singular Ag(001) substrates held at room temperature, as described previously.[14,20] Room temperature growth is necessary for minimizing interdiffusion and results in high-quality interfaces and well-defined magnetic anisotropies. For films above 5 ML thickness prepared in this way, the samples have an in-plane easy axis, as required for the PNR measurements. The use of singular substrates is important in view of the previous PNR studies, which show that vicinal substrates can introduce significant diffuse scattering. Moreover, the vertical mismatch between the bcc Fe and fcc Ag lattice parameters makes the growth very sensitive to the presence of steps on the surface, making the use of singular substrates important.[20,24] The in-plane lattice parameter was determined from RHEED measurements during growth as in previous studies. Very reproducible intensity oscillations were observed, and the Fe-layer thickness was determined from the period of oscillation, which was correlated with the output of a thickness monitor. The period determined for thickness beyond 6 ML was used, since a gradual change in periodicity is observed during the growth of thicknesses up to 5 ML. Samples were terminated at the maximum RHEED intensity in each case. The thickness of the film is estimated to be reproducible to within 0.2 ML. Thinner films were not prepared for this study because of the difficulty of reliably estimating the film thickness during the early stages of Fe layer growth. RHEED patterns and RHEED intensity oscillations indicate that the interface roughness is limited to a maximum of two monolayers.[18–21] The Ag-coated 10.9 ML Fe sample (see Table I) was prepared as a reference sample, since an average moment per atom close to the bulk value can be expected for this thickness.[2,10] The comparison of the moment for this sample with that of thinner samples prepared in the same way provides a crucial test of the theoretical prediction that significantly enhanced moments occur in the vicinity of the film interfaces. We shall also include a discussion of a previously studied Au-coated 9 ML Fe film[11] listed in Table I. Near identical second versions of the Cu/Fe and Pd/Fe samples were prepared as a test of the reliability of the PNR measurements. The complete set of samples with similar Fe-layer thickness permits the effect of the overlayer to be systematically studied. All samples were protected with a final Au capping layer. In the first version of each sample, thicker Au capping layers were used (24–52 ML) than in the second versions (20 ML). In referring to the samples in the rest of this paper, all thicknesses are given in ML.

III. POLARIZED-NEUTRON REFLECTION

The PNR technique has been demonstrated to provide an accurate means of determining the absolute value of the magnetization of ultrathin films with no contribution to the spin-dependent reflectivity requiring correction arising from the substrate.[15] In PNR the partially reflected neutron intensity is measured as a function of the incident spin state and incident wave vector, as shown schematically in Fig. 1. The incident wave vector $\mathbf{k}_i$ is varied either by rotating the sample with fixed incident wavelength λ_i or by employing a time-of-flight method with a fixed incidence angle θ_i.[15] Such measurements typically permit the refractive index profile of the solid medium to be determined with a depth resolution in the nm range. For ultrathin films, the spatially averaged magnetic moment can be determined. We first outline the theory of PNR as a magnetometric technique applied to perfect ultrathin films. A detailed account of the experimental methods is given elsewhere.[15]

A. Ideal interfaces

The reflecting (ferromagnetic) medium can be ideally represented by a one-dimensional optical potential $V(y)$, where the direction normal to the surface of the film defines the y axis. A multilayer can be described by a sequence of layers (i.e., a stratified medium), each with a constant interaction potential. For the ith layer, the in-plane spatially averaged optical potential V_i, may be approximated by

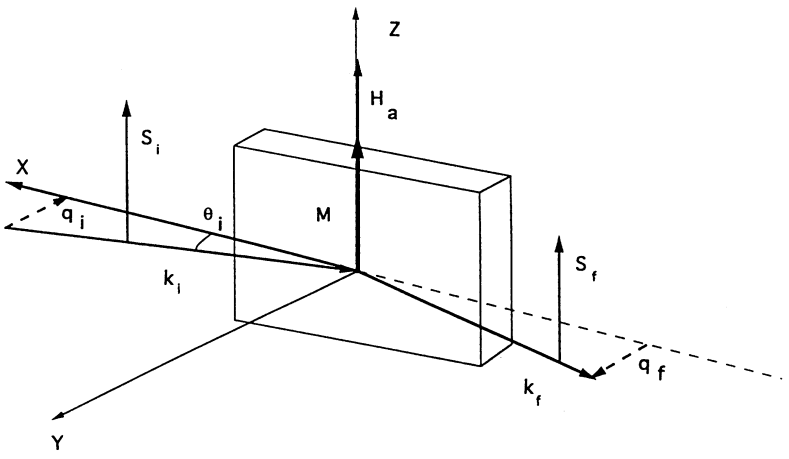

FIG. 1. (a) The geometry for PNR from a single interface. The neutron wave is incident at a grazing angle θ_i from the solid medium (rectangular box) as shown schematically with x,y the scattering plane (see text). The incident perpendicular wave-vector component is given by $q_i = k\sin(\theta_i)$. The reflected beam has a wave vector $\mathbf{k}_f$ with a perpendicular component q_f equal in magnitude to the incident perpendicular wave-vector component. The incident and final spin states $\mathbf{S}_i, \mathbf{S}_f$ are parallel (or antiparallel) to the applied field $\mathbf{H}_a$ and the sample magnetization $\mathbf{M}$, which is assumed to lie parallel to $\mathbf{H}_a$. Away from the sample the spin polarization is maintained by a weak guide field $\mathbf{H}_g$ (not shown) directed along the incident spin direction.

$$V_i = \frac{2\pi\hbar^2}{m_n}\rho_i b_i - \mu_n \cdot \mathbf{B}_i \ , \tag{1}$$

where m_n is the neutron mass, ρ_i is the atomic density, b_i is the bound coherent neutron-scattering length of the material,[15] μ_n is the neutron magnetic moment, $\mathbf{B}_i$ is the total magnetic induction in the medium (arising from the magnetically aligned atomic moments), and the suffix i labels the medium. The medium is assumed to be a saturated ferromagnet with the spins in plane. Nonmagnetic media have no magnetic term. The perpendicular wave-vector component (i.e., along the y direction) of the neutron is given for the jth medium by

$$q_j = \sqrt{q_i^2 + q_{ci}^2 - q_{cj}^2} \tag{2}$$

and with the critical wave vector q_{ci} for the ith medium given by

$$q_{ci}^2 = \frac{2\mu_n}{\hbar^2} V_i \ . \tag{3}$$

Total reflection, therefore, occurs for $q_i^2 < q_{cj}^2 - q_{ci}^2 = k^2 \sin^2\theta_{cij}$, where θ_{cij} is the critical angle for the i,j interface. The spin-dependent critical angle is given by

$$\sin^2\theta_{cij}^{\pm} = \frac{4\pi}{k^2}(\rho_j b_j^{\pm} - \rho_i b_i^{\pm}) \ , \tag{4}$$

where we have introduced the spin-dependent effective scattering length:

$$b_i^{\pm} = b_i \pm c\mu_i \tag{5}$$

with the signs corresponding to the neutron spin parallel $(+)$ or antiparallel $(-)$ to the magnetization, where $c = (m_n/2\pi\hbar^2)\mu_B\mu_n = 0.2695\times10^{-15}$ m, and μ_i is the moment per atom of the layer in Bohr magnetons. The solution to Schrödinger's equation for the optical potential of Eq. (1) for the ith medium is given by the sum of a forward and backward traveling wave:

$$\psi_i(y) = A_i \exp[iq_i(y - y_0)] + B_i \exp[-iq_i(y - y_0)] \ . \tag{6}$$

Applying the boundary condition that the wave function and its derivative are conserved at each interface permits the reflection and transmission coefficients $r_{12,\ldots,N}, t_{12,\ldots,N}$ to be calculated for a multilayer system composed of media $1,\ldots,N$ as indicated by the subscripts. Matrix methods for calculating these coefficients have been described elsewhere.[25] It is also straightforward to follow an approach frequently used in multilayer optics in which the amplitude of successively reflected beams is added in a geometric series.[26] As an example, we consider a three medium system with the wave incident from the first medium. Defining $A_1 = 1$ and $B_1 = r_{123}$ (i.e., the forward and reflected wave amplitudes in the first medium), we obtain the following expression for r_{123}:

$$r_{123} = \frac{r_{12} + r_{23}\phi_2}{1 + r_{12}r_{23}\phi_2} \ , \tag{7}$$

where the reflectivity for the single ij interface is given by

$$r_{ij} = \frac{q_i - q_j}{q_i + q_j} \ , \tag{8}$$

where $\phi_2 = \exp(2iq_2d_2)$ and d_2 the thickness of the second layer. The transmission coefficient t_{ij} for the interface is readily obtained from Eq. (8). Having obtained a similar expression for r_{ijk}, we can write down an iterative expression for the reflectivity of a four-medium system in terms of r_{12} and r_{234}. This approach can be extended to an arbitrary number of layers, and the reflectivity can be computed for each spin state separately.

In PNR, the intensity reflectivity $R^{\pm} = |r^{\pm}|^2$ is measured as a function of the incident spin state. The flipping ratio $F = R^+/R^-$ or the spin asymmetry $S = (F-1)/(F+1)$ is determined as a function of the wave vector in order to probe the ferromagnetic response of the sample and from which magnetometric information can be obtained. In the absence of ferromagnetism $F = 1$ and $S = 0$. For the case of a ferromagnetic film of monolayer range thickness supported by a thick nonmagnetic substrate, the spin asymmetry is often small, and in-

creases approximately quadratically with a perpendicular wave vector.[15] By overcoating the ultrathin ferromagnetic film with a nonmagnetic layer of appropriate thickness, the sensitivity of the spin asymmetry to the layer magnetization at low wave vector is enhanced due to a neutron-optical interference effect, resulting in a peak in the spin asymmetry at a low wave vector.[25,27] In the region of the peak spin asymmetry, the form of S as a function of the wave vector is to a first approximation independent of the ultrathin magnetic layer thickness for a symmetrically sandwiched ultrathin-film structure. Hence, similarly shaped curves are obtained for films of different magnetic moment, as confirmed experimentally. The value of the spin asymmetry at the first peak yields the total magnetic moment of the layer, while the overlayer thickness can be determined from the wave-vector position at which the peak occurs. By comparing the observed spin asymmetry with that calculated exactly for the sandwich structure, it is possible to extract the value of the total magnetic moment of the ferromagnetic layer when it is magnetically saturated in plane. An accurate estimate of the magnetic moment per atom $\mu_3 = g s_3 \mu_B$ ($g = 2$) can then be obtained independently of the perpendicular lattice parameter, provided the in-plane lattice parameter of the film and its thickness in ML is known. All other relevant parameters required can be obtained by fitting the reflectivity data over a sufficiently large wave-vector range.

B. Interface roughness

In real surfaces, the interface is never flat, but, in describing the effect of interface fluctuations upon the neutron reflectivity, it is first necessary to consider the length scale over which the fluctuations occur. Macroscopic surface waviness gives rise to long-range fluctuations in the surface flatness, i.e., the fluctuations are correlated over a distance much longer than the effective coherence length of the neutron in plane [typically 100 μm (Ref. 15)]. Such waviness can be described by an increase in the effective wave-vector resolution of the experiment, equivalent to an increase in the angular spread of the incident beam. Steps, mosaic spread, dislocations, macroscopic defects of the substrate, etc., give rise to fluctuations correlated over a distance short on the length scale of the effective coherence length of the neutron in plane. The condition for optical interference to occur requires that the fluctuations δt are small on the scale of the perpendicular wavelength, i.e., $\delta t \ll 0.02$ μm for cold neutrons ($\lambda \sim 10$ Å).

Nevot and Croce[28] showed that, for x rays reflected from an interface exhibiting a random Gaussian roughness distribution, the specular reflectivity r_{ij} is modified to become $r_{ij} \exp(-W_{ij})$, where $W_{ij} = 2 q_i q_j \sigma_{ij}$ and where $\sigma_{ij} = \langle \Delta y_{ij}^2 \rangle$ defines the variance of the local fluctuation in interface position Δy_{ij} given by $\Delta y_{ij} = y_{ij} - \langle y_{ij} \rangle$, where the angular brackets indicate averaging over in-plane positions. In practice, roughness correlations occur due to such features as steps, terraces, etc., and the correlation function $e(r_\parallel)$ defined as $\langle \Delta y_{ij}(r_\parallel) \Delta y_{ij}(0) \rangle$ (where the angular brackets indicate averaging over radial position $r_\parallel$ in-plane) is now nonzero, and diffuse reflection occurs. The diffuse scattering process in reflection has been considered by several authors for light[29] and also for x rays and neutrons.[30] The wave incident at a glancing angle θ_i is refracted but is subsequently scattered from an impurity or defect within the vicinity of the interface. This gives rise to an scattered beam which emerges at a general angle θ_f with respect to the interface.

We assume, following Steyerl[31] that the roughness spectrum is Gaussian and short ranged and therefore can be described in terms of a roughness amplitude $\sigma^{1/2}$ and a correlation length w. At a large wave vector, the diffuse scattering as a function of the scattering angle θ_f has the form of a Gaussian centered at the specular position with an angular width $\Delta\theta_f$ given by approximately $1.4/kw$ (Ref. 31) and so yields a direct estimate of the correlation length of the roughness fluctuations. In epitaxial films, roughness coherence lengths in the range 100–500 Å are typical, corresponding to angular widths of the order of 5–25 mrad. These widths exceed the angular spread of the incident beam (3 mrad) and are therefore easily measurable. The broadening of the RHEED specular spot indicates that the mosaic spread is around 5–9 mrad in good vicinal Ag substrates and therefore that the mosaic spread may influence the beam profile in PNR.

In order to fit the profile, the scattered intensity $I(q_f)$ is assumed to be of the form

$$I(q_f) = \int_{q_f - \Delta q_i/2}^{q_f + \Delta q_i/2} I(q_i) R(q_i) \exp(-2W) dq_i + \frac{I_0}{A_b} \left[\frac{d\sigma^d}{d\Omega} \right] \Delta\Omega , \quad (9)$$

where the first and second terms are the roughness modified specularly and diffusely reflected intensities, respectively. The factor $\exp(-2W)$ describes the overall reduction in reflectivity of the entire structure computed for randomly rough interfaces,[28] $\Delta\Omega$ is the solid angle subtended by the detector, I_0 is the total intensity of the beam incident upon the sample (integrated over the range of incident wave vectors), and A_b is the usable beam cross-sectional area. The function $I(q_i)$ describes the incident intensity distribution as a function of wave vector and the second term describes the diffuse scattering intensity accepted by the detector.[13] In the present work, following a procedure first described in Ref. 13, we fit the background-corrected reflected beam profile to the sum of two components: (i) a "specular" component with the line shape of the incident beam determined at very low q and (ii) a "diffuse component" with a Gaussian shape and a width $(\Delta q)_{\text{diff}}$. At very low q ($q < q_c$) diffuse scattering is negligible in comparison with the strong specular reflection, and hence the line shape here can be used to determine the specular component. The diffuse scattering is determined by treating the intensities of these two contributions as adjustable parameters and the width $(\Delta q)_{\text{diff}}$ as a third adjustable parameter. Since $(\Delta q)_{\text{diff}}$ exceeds Δq the "wings" of the measured profile can be

used to determine the diffuse component. This procedure provides a three-parameter fit to the observed line shape for each incident q. Thus we obtain R, w, and the diffuse cross section $(d\sigma/d\Omega)$ in the specular direction for each value of q. The specular component is not necessarily of the same shape as the incident line shape, since macroscopic surface waviness can cause broadening. In fitting the wave-vector width of the specular component Δq, the profile obtained at small wave vector ($q < q_c$) is used. Distortion of the beam profile occurs when the average incident wave vector is sufficiently close to the critical angle that a significant part of the incident wave-vector spectrum is reflected critically from the sample. Therefore, for incident wave vectors close to the critical value, the resulting profile cannot be used to estimate the width of the specular component.

C. Experiment

The PNR measurements were carried out at the Institut Max von Laue–Paul Langevin (ILL), Grenoble on the D17 diffractometer using the rotating-sample method described above with samples of area ~ 2 cm^2. The incident beam has an angular divergence $\Delta\theta = 3\times10^{-3}$ rad and a wavelength λ is fixed at 12 Å, defined to within 10%, giving an overall full width at half maximum of the incident beam with $\Delta q \sim 6.7\times10^{-4}$ Å^{-1}. The reflected and transmitted beams are measured using a BF_3 128×128 pixel multidetector positioned at 2.83 m from the sample. In determining the reflected intensity, the intensities of a group of pixels in the vicinity of the specular beam are binned to improve the signal-to-noise ratio. Accordingly, the number of pixels used determines the solid angle accepted. A solid angle of 7×10^{-6} sterad was used in determining the spin asymmetry for the samples with 20 ML Au capping layers, with the exception of the Au/9 Fe reference sample. For other samples, solid angles in the range $(2-2.8)\times10^{-5}$ sterad were used in determining the spin asymmetry. The incident beam polarization was in the range 84–87% for all measurements reported here. A summary of the experimental parameters used for each sample is given in Table I. Before analyzing the intensity, the background is subtracted and the detected signals corrected for the incident beam polarization.[15] The measured spin asymmetry S_m is corrected for the beam polarization P_0 using the relation

$$S = \frac{S_m}{P_0} . \tag{10}$$

In all cases, the spin asymmetry is corrected for the diffuse scattering present in the detected beam. Spin-dependent reflectivity measurements $R^{\pm}(q)$ were made in the reduced wave-vector range $0.5 < q/q_c < 3.5$. For the magnetic moment measurements, the samples were held at a temperature in all cases less than 20 K. Total counting times per q scan of 12–24 h were used with the counting time per point increased for high wave vectors. The samples were magnetically saturated along the easy axis in plane using an applied field of 800 G collinear with the guide field as described above. For temperature-dependent measurements, the temperature was uniformly ramped under computer control from 10–300 K in 12 h, and the spin asymmetry was determined at a fixed wave vector close to $1.5q_c$. In this way the relative magnetization was determined as a function of temperature.

D. Diffuse scattering measurements

The separation of the diffuse and specular contributions using the fitting procedure described in Sec. III B reveals that diffuse scattering from microroughness has a significant effect upon the measured reflectivity. As an example of the effect of the diffuse scattering, we consider the beam profile observed for the Ag/5.5 Fe sample. In Fig. 2(a) the detected raw intensity is plotted as a function of the scattered wave vector for four values of incident wave vector. The large peak centered at $q_f = 0$ in each panel corresponds to the directly transmitted beam. As the incident wave vector is increased, the reflected beam (the second peak) moves to larger values of the scattered wave vector, and changes in line shape are observed. The reflected beam at $q_i = 0.85q_c$ provides an estimate of the effective specular width of $\Delta q = 0.2q_c$. The increase in the width of the reflected peak at $1.12q_c$ is due to the beam-distortion effect in the vicinity of the critical edge described in Sec. III B. However, at large incident wave vectors the effects of diffuse scattering are apparent: the width of the reflected peak is significantly broader for $2.72q_c$ than for $2.07q_c$. The procedure for separating the specular and diffuse contributions to the observed reflected intensity is illustrated in Fig. 2(b) for $q_i = 2.6q_c$. The background (dashed line with squares) is estimated from a separate measurement with the sample turned away from the reflecting position. The diffuse intensity (dashed line) is modeled as a Gaussian curve, centered on the specular position ($2.6q_c$) with a width and intensity that fits the measured intensity in the wings of the peak. In this way the diffuse width is estimated as $(\Delta q)_{\text{eff}} \sim 0.4q_c$ and the diffuse intensity is found to be approximately 50% of the total intensity at this value of incident wave vector. The total contribution (the background intensity plus diffuse scattering plus the specularly reflected component) is shown as a continuous line, and the total measured intensity is shown as solid circles. The diffusely reflected intensity is found to be $\sim 8-10\%$ of the overall signal at $q \sim 1.5q_c$ for a detector solid angle $\Delta\Omega \sim 2.8\times10^{-5}$ sterad.[32] This diffuse contribution rises rapidly to $\sim 20\%$ and $\sim 80\%$ for $q \sim 2q_c$ and $q \sim 3q_c$, respectively until at $q \sim 3.5q_c$ virtually all that is measured is the diffusely reflected intensity scattered in the specular direction. The presence of such strong diffused scattering complicates the fitting of the reflectivity. Assuming similar levels of roughness at each interface, we estimate $\sigma^{1/2} = 14\pm4$ Å and $w = 198\pm20$ Å for the sample from the fitted diffuse scattering. The interface roughness and correlation length has been determined in the same way for all the samples studied, and comparable values are found in each case—see the summary given in Table I. This is consistent with the reproducible structural and magnetic properties of the samples. A mean distance of 50–60 Å between the top atomic terraces is determined from RHEED studies using the same growth conditions

used in the samples investigated here. For samples prepared with part of the Fe growth carried out at elevated temperature, average terrace widths of the order of 400 Å are determined.[33] It should be noted that while the effective coherence length of the roughness determined by PNR is model dependent and cannot be exactly equated with the separation between the top atomic terraces, the present study suggests that these quantities are of the same order of magnitude as might be expected. RHEED studies of the roughness of Fe grown at room temperature indicate that a maximum of two Fe layers are partially filled, suggesting that the rms roughness on a local scale is of the order of 1 Å. A conversion electron Mössbauer spectroscopy (CEMS) study on equivalent samples confirm that the Fe/Ag interface consists of atomic terraces, one atomic layer in height with an average terrace edge of 4 nm.[34]

The large roughness amplitude deduced from the PNR data might be thought to suggest that the film interface is ill defined, in contrast with the results of the RHEED and CEMS studies. Clearly interference of the neutron wave within the structure would not occur if this were

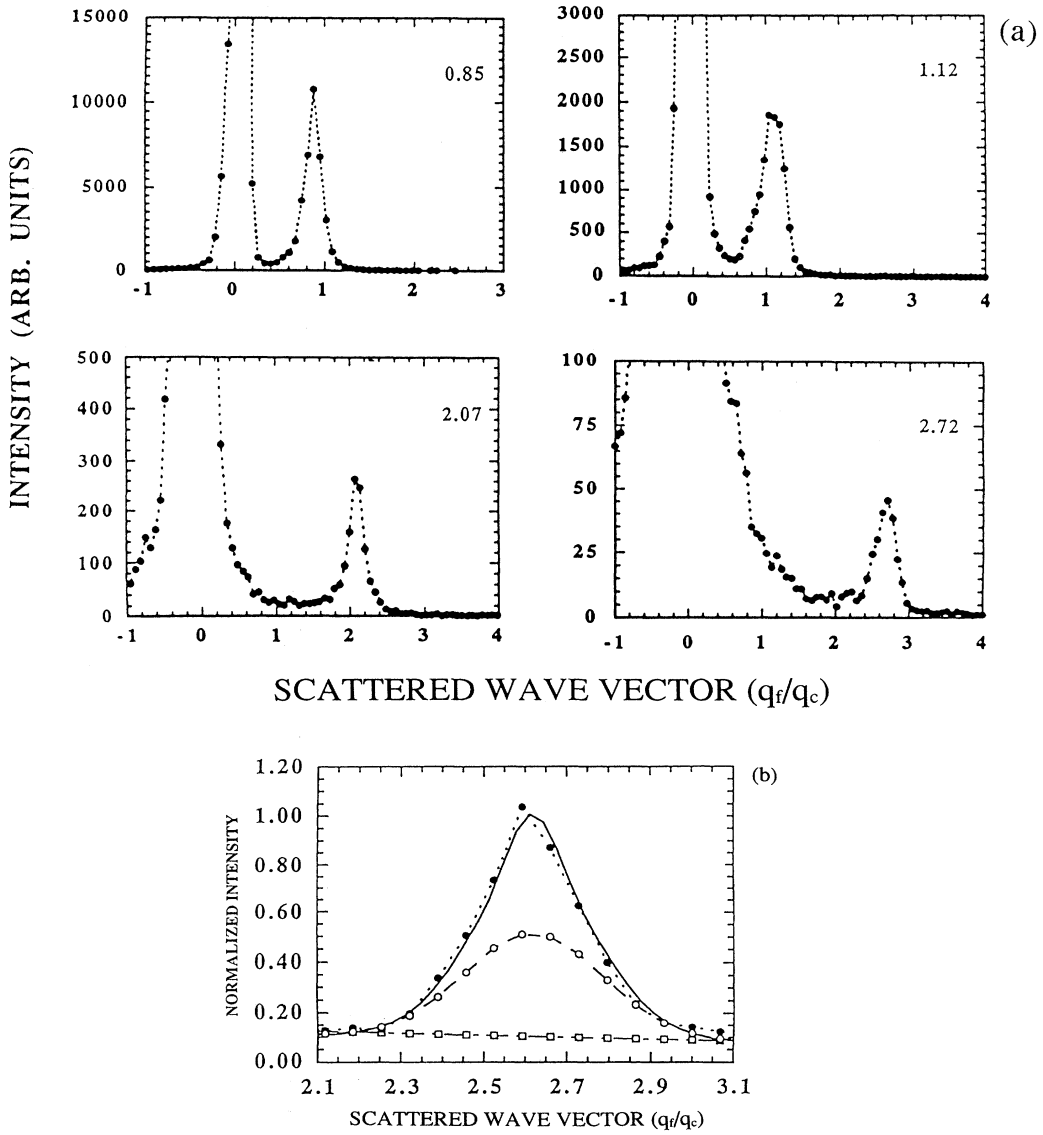

FIG. 2. (a) The measured beam profile for the Au/Ag/5.5-ML Fe/Ag sample (referred to in the text) as a function of a scattered perpendicular wave vector q_f for values of the incident wave vector q_i of $0.85q_c$, $1.12q_c$, $2.07q_c$, and $2.72q_c$. At small q_i the beam profile is similar to that of the incident beam, showing that the sample surface is reasonably flat. At larger incident wave vectors, the reflected beam contains an increasing component due to diffuse scattering associated with interface inhomogeneities. (b) The reflected beam profile of the Au/7-ML Ag/5.5-ML Fe/Ag(001) sample for $q=2.6q_c$ as a function of reduced final (scattered) wave vector q_f/q_c. The measured data (filled circles), the background (dashed line plus squares) and the diffuse contribution (open circles) are shown. The fit to the data is shown as a solid line.

the case. The key to reconciling these data is to note that the interface roughness is determined on different lateral length scales in the PNR and RHEED experiments and that these length scales differs by several orders of magnitude. The value for the roughness amplitude in PNR corresponds to an effective value associated with the variations in the surface of the substrate over the size of the effective neutron coherence length in plane (100 μm), but on a local scale of <500 Å (as probed by short-coherence-length probes such as RHEED) the interface is indeed atomically sharp. Because the neutron beam probes a very large area, it is likely that macroscopic scratches influence both the apparent roughness coherence length and amplitude. One, therefore, cannot expect an exact correspondence between the roughness determined by PNR and that determined by RHEED. We can consider the average inclination angle that the surface roughness defines in both cases. If we have two partially covered atomic layers, as suggested by the RHEED data, and the separation between the top atomic terraces is $w_s = 60$ Å, then the average inclination angle is given by $2d/w_s = 0.05$ rad, where $d = 1.435$ Å is the Fe interlayer separation. This angle is close to the ratio of the roughness amplitude to the coherence length determined by PNR, $\sigma^{1/2}/w = 0.07$ rad, as might be expected.

In an independent study of the interface roughness, high-resolution x-ray-diffraction measurements were carried out on equivalent samples.[23] In fitting the data, the scattering factor is averaged over in-plane dimensions in which coherent scattering occurs and random discrete fluctuations in the substrate height and layer thickness are assumed with different regions of the film having different vertical configurations. The results are consistent with layer fluctuations confined predominantly to one monolayer about the average thickness with typically seven regions of different thickness and/or substrate height contributing to the coherent intensity. Thus it is likely that variations in substrate height are responsible for the large effective roughness probed in PNR.

We now need to consider the effect of the diffuse scattering upon the spin asymmetry. In the presence of a diffuse reflection R_D the measured spin asymmetry $S_m(q)$ can be written as

$$S(q)=\frac{(R_s^+ + R_D^+ - R_s^- - R_D^-)}{(R_s^+ + R_D^+ + R_s^- + R_D^-)} . \tag{11}$$

While the diffuse reflectivity accepted by the detector strongly perturbs the reflectivity curves, the effect upon the spin asymmetry is much weaker, since the spin asymmetry has a spin dependence R_D^+/R_D^- close to that of the specular reflectivity. Thus, while for example the intensity contribution of the diffuse scattering is of the order 50% at $2.6q_c$ in Fig. 2(b), the corresponding effect of the diffuse scattering on the spin asymmetry is much smaller, although still significant. In our samples, the spin asymmetry of the diffuse scattering is found to be slightly *smaller* than that of the true specular asymmetry, and to slightly vary with scattering angle. As a result, it can be seen from Eq. (11) that the diffuse scattering reduces the spin asymmetry by a factor dependent on the solid angle used. For the Ag/5.5 Fe sample the diffuse scattering contribution to the reflected intensity accepted by the detector using a detector solid angle of $\Delta\Omega \sim 1.4\times10^{-5}$ sterad is found to lower the peak spin asymmetry by ~ 5–6%. Such a correction is, therefore, significant in determining the magnetic moment. For the smaller solid angle of $\Delta\Omega \sim 7\times10^{-6}$ sterad, the corresponding correction is $\sim 2\%$. The correction is small because the diffuse scattering strength relative to the specular intensity falls as the acceptance is reduced. In an earlier PNR study, the asymmetry was studied for a Ag/8-ML Fe sample prepared on a vicinal Ag(001) crystal surface.[16] The diffuse scattering is strong enough in this case to very strongly perturb the reflected beam profile at intermediate wave vectors.[35] The moment estimated from the total reflected signal accepted by the detector at the specular position was strongly reduced from the bulk value.

IV. GROUND-STATE MAGNETIC MOMENTS

In Fig. 3 we show the observed spin asymmetry (solid circles) corrected for partial incident beam polarization,

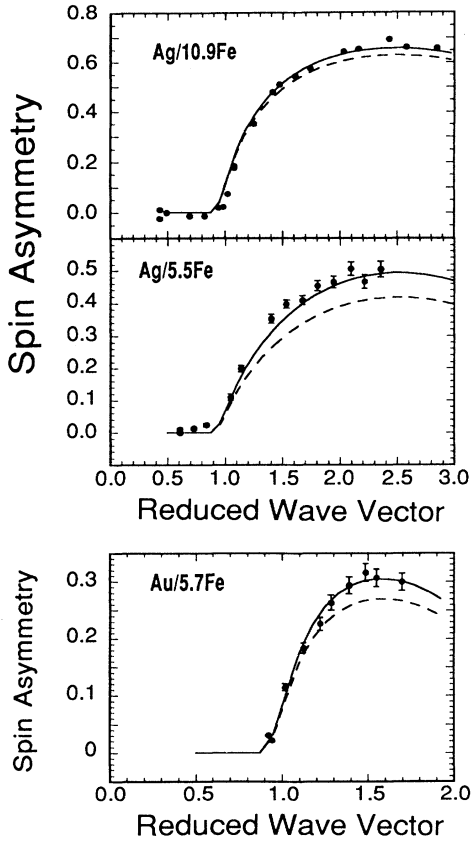

FIG. 3. The corrected spin asymmetry obtained at low temperature for (top panel) 20-ML Au/7-ML Ag/10.9-ML Fe/Ag(001), (middle panel) 20-ML Au/7-ML Ag/5.5-ML Fe/Ag(001), and (bottom panel) 52-ML Au/5.7-ML Fe/Ag(001). The dashed and solid lines in the plots of the spin asymmetry refer to model fits for the bulk moment and assuming an enhanced moment, respectively (see text).

background intensity, and diffuse scattering for the Ag/Fe and Au/Fe samples. In each case the spin asymmetry is calculated assuming uniformly magnetized ferromagnetic layers with a moment per atom adjusted to best fit the data (shown as a solid line) and also assuming the bulk value of $\mu_{Fe}=2.2\mu_B$ (shown as a dashed line). We have also assumed that no spin polarization is induced in the Ag substrate. In fitting the asymmetry the nuclear scattering lengths appropriate to the bulk materials and the experimentally determined values of lattice parameter and layer thickness are assumed for all samples. The degree of strain in the layers is sufficiently small for bulk densities to be assumed in all cases. This assumption is well justified, since x-ray-diffraction studies[23] confirm that the Fe lattice spacing is very close to the bulk value and that the Pd atomic volume is constant to better than 1% despite a perpendicular lattice contraction of 7.2%. The only variable parameters are therefore the layer-dependent magnetization and the roughness amplitude. However, the spin asymmetry is insensitive to small roughness amplitudes and so the spin asymmetry can be fitted with the magnetic moment the only adjustable parameter. For samples for which a small detector acceptance angle was used, the asymmetry is well fitted in the vicinity of the enhancement peak although the fit is less good at smaller wave vectors, possibly due to beam distortion. By comparing the observed asymmetry with that calculated for $\mu_{Fe}=2.2\mu_B$ we see the moment is clearly enhanced in all cases with respect to the bulk value. The error in thickness determination is in this case small (around 4%). It should also be noted that since the magnetic moment is directly determined in PNR it is sufficient to know the magnetic layer thickness in ML (as yielded by RHEED) rather than in absolute units. This is because the perpendicular lattice constant is canceled in the product $\rho_i d_i$. The wave vector spread of the incident beam $\Delta q_i=0.16q_c$ has a negligible effect on the spin asymmetry except at $q_i=q_c$, where a rounding of the reflectivity is observed.

The spin asymmetry for the Ag/10.9 Fe reference sample corrected for diffuse scattering is shown at the top of Fig. 3. It can be clearly seen that the spin asymmetry is higher than that predicted for the bulk moment, although the degree of enhancement is very small due to the large thickness of the film. The layer-averaged moment per atom is estimated to be $\mu_{Fe}=(2.33\pm0.05)\mu_B$ from the variation of χ^2. In the vicinity of the critical wave vector, the effect of the wave-vector spread is apparent, and this has been modeled in the simulation. The fitted moment for the Ag/10.9 Fe sample is very close to the previously reported value of $2.3\pm0.1\mu_B$ obtained without correction for the diffuse scattering.[12] The close agreement is due to the small solid angle (7×10^{-6} sterad) used in this case. The present result illustrates that the accuracy of the PNR method is of the order of $0.1\mu_B$ per atom for appropriate samples. A significant aspect of the data is that for wave vectors beneath the critical value the spin asymmetry is zero within experimental error, as expected. This contrasts with the anomalous dip in the uncorrected spin asymmetry that occurs in the critical region for a Ag/8 Fe sample prepared on a vicinal Ag substrate.[16] Calculations show that the diffuse scattering is strongest for the (−) spin state, assuming roughness localized at the substrate interface, giving rise to a negative spin-asymmetry dip in the critical region, as observed.

The spin asymmetry, corrected for diffuse scattering, for the Ag/5.5 Fe sample is shown in Fig. 3 (central panel). By varying the moment, it is concluded that $\mu_{Fe}=2.58\pm0.09\mu_B$ provides the best estimate of the layer-averaged moment per atom for the Ag/5.5 Fe/Ag sample. The calculations of Ohnishi, Weinert, and Freeman[8] for a Ag/5 Fe/Ag(001) sandwich structure predict a moment of $0.08\mu_B$ for the first Ag layer, which is too small to be determined in the present experiments, and a layer-averaged moment per Fe atom of only $2.4\mu_B$, which is significantly smaller than the enhanced value we observe. Comparable values of the layer-averaged moment per atom are also expected for Fe layers overcoated with Au.[9] The calculations predict a significantly enhanced moment for the interface Fe layer for Ag and Au sandwiches, but our measurements do not extend sufficiently far in the wave vector to allow direct observation of the predicted magnetization profile. Both results are, however, consistent with a moment per Fe atom at the Fe/Ag interface of about $2.5\mu_B$ and a moment per atom close to the bulk value in the film center, as predicted theoretically. The comparison between samples, therefore, provides important evidence that the enhancement is associated with the presence of the interfaces, as predicted by theory.

The ratio of the magnetization of the Ag/5.5 Fe to the Ag/10.9 Fe samples was determined to be 1.06 ± 0.02 by FMR, which can be compared with the value of 1.11 ± 0.04 determined by PNR. The relative increase of the moment of the Ag/5.5 Fe sample with respect to the Ag/10.9 Fe reference sample provides conclusive evidence for the increase of the moment with reduced thickness, while the PNR measurements show that in both cases the absolute value of the moment is enhanced with respect to the bulk value, yielding a ratio in agreement with that deduced by FMR within experimental error. FMR measurements of the relative magnetization with respect to a Au/5.7 Fe sample were reproducible to 2% accuracy for all the samples shown in Table II. To enable a direct comparison, the values of the moment determined by PNR with respect to this sample are also shown. It should be noted that the PNR results provide a more accurate value for the magnetic moment than for the ratio of moments between samples: an overall accuracy of ±3% is obtained for the absolute moment of the Ag/5.5 Fe sample. FMR does not yield the absolute value of the moment of the sample.

In Fig. 3 (bottom panel) we show the spin asymmetry for the Au/5.7 Fe sample corrected for diffuse scattering. A best-fit value of $2.5\pm0.1\mu_B$ obtained although the accuracy achievable on this sample was reduced by using a larger solid angle on the detector (see Table I). Significant diffuse scattering occurred in this sample, requiring correction in the spin asymmetry. A previously investigated Au/9 Fe reference sample yielded an estimated moment of $2.3\pm0.2\mu_B$ when corrected for diffuse scattering.[11] The large error in this case is due to

TABLE II. The magnetic and structural parameters of the bcc Fe/Ag(001) sandwich structures defined in the first column. The second column gives the value of the Fe-layer magnetic moment used in fitting the spin-asymmetry data. The third column gives the ratio of the layer-averaged moment per Fe atom estimated by PNR to the bulk moment ($2.22\mu_B$). The fourth column lists the ratio of the moment per atomic layer for the sample scaled by that of a 20 Au/5.7 ML Fe/Ag(001) reference sample as determined by FMR at 77 K, and the fifth column gives the corresponding value estimated from the PNR measurements at low temperature. The sixth column lists the in-plane anisotropy strength determined by FMR. The seventh column lists the value of $4\pi M_{\text{eff}}$ as measured by FMR.

Sample (Thicknesses in ML)	μ_{Fe} (μB)	$\frac{\mu_{\text{Fe}}}{\mu_{\text{bulk}}}$	$\frac{M_{\text{FMR}}}{M(5.7)}$	$\frac{M_{\text{PNR}}}{M(5.7)}$	$\frac{2K_1}{M_S}$ (kOe)	$4\pi M_{\text{eff}}$ (kOe)
20 Au/7 Ag/5.5 Fe/Ag(001)	2.58±0.09	1.16±0.04	0.99±0.01	1.03±0.05	0.218	1.21
20 Au/7 Ag/10.9 Fe/Ag(001)	2.33±0.05	1.05±0.02	0.93±0.01	0.93±0.05	0.544	7.06
52 Au/5.7 Fe/Ag(001)	2.5±0.1	1.13±0.05	1.00	1.00	0.255	7.44
20 Au/9 Fe/Ag(001)	2.3±0.2	1.03±0.09			0.479	9.702
20 Au/7 Cu/5.8 Fe/Ag(001)	2.48±0.08	1.12±0.04	1.02±0.01	0.99±0.05	0.325	0.94
42 Au/8 Cu/5.7 Fe/Ag(001)	2.5±0.1	1.13±0.05		1.0±0.06	0.378	0.91
20 Au/7 Pd/5.6 Fe/Ag(001)	2.66±0.05	1.20±0.02	1.03±0.01	1.06±0.04	0.223	10.91
42 Au/8 Pd/5.7 Fe/Ag(001)	2.6±0.2	1.17±0.09	1.044±0.01	1.04±0.09	0.225	9.87
24 Au/3 Ni/5 Fe/Ag(001)	2.6±0.1[a]	1.17±0.05		1.04±0.06	0.212	8.30

[a]This value for the Fe moment assumes that the Ni moment is close to the bulk value of 0.6 Bohr magnetons (Ref. 11).

significant diffuse scattering resulting from the large solid angle used. These combined results for the Au/Fe interface nonetheless confirm the same thickness dependent trend observed for the Ag/Fe interface.

In Fig. 4 (left-hand panels) the spin asymmetry corrected for diffuse scattering is shown for the Cu/5.8 Fe and Pd/5.6 Fe samples measured at high detector resolution. A strong enhancement of the moment is observed in each case. Best-fit values of the layer-averaged moment of $2.48\pm0.08\mu_B$ and $2.66\pm0.05\mu_B$ are determined for the Cu/5.8 Fe and Pd/5.6 Fe structures, respectively, where we have assumed that no induced polarization occurs in the interface Pd layers. These values agree closely with the previously reported values of $2.5\pm0.1\mu_B$ and $2.6\pm0.1\mu_B$, respectively, obtained without correction for the diffuse scattering using a small detector angle.[12] The best-fit values are seen to reproduce the data quite well within experimental error, although in the case of the Cu/5.8 Fe sample, some reduction at a high wave vector occurs with respect to the overall best-fit values. For the Cu/5.8 Fe sample, the effect of the wave-vector spread is not included in the fits shown in the figure, and, for the Pd/5.6 Fe sample, the effect of the wave-vector spread is not shown for the bulk moment simulation. Omitting the effect of the wave vector spread does not significantly affect the fit away from the critical region.

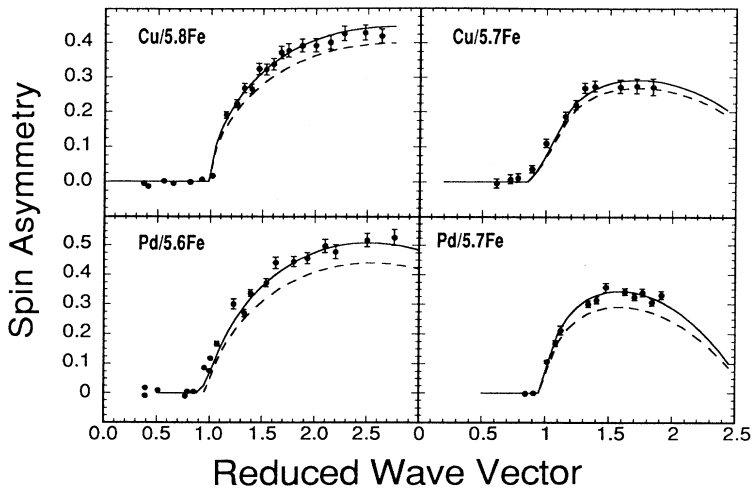

FIG. 4. The corrected spin asymmetry obtained at low temperature for (top left panel) 20-ML Au/7-ML Cu/5.8-ML Fe/Ag(001), (bottom left panel) 20-ML Au/7-ML Pd/5.6-ML Fe/Ag(001), (top right panel) 42-ML Au/8-ML Cu/5.7-ML Fe/Ag(001), and (bottom right panel) 42-ML Au/8-ML Pd/5.7-ML Fe/Ag(001). The dashed and solid lines in the plots of the spin asymmetry refer to model fits for the bulk moment and assuming an enhanced moment, respectively (see text).

The reproducibility of the PNR measurements for these samples can be assessed from the results of separate experimental investigations at low detector resolution for the Cu/5.7 Fe and Pd/5.7 Fe second version samples. These samples also permitted the question of the structures best suited to PNR measurements to be addressed, since a total overlayer thickness closer to 50 ML was used (see Table II). In these versions the degree of surface flatness is in several cases poorer, as judged by the form of the reflectivity as a function of the wave vector in the vicinity of the critical angle. This required using a larger angular acceptance in the detector (see Table I). The spin asymmetries are shown in Fig. 4 (right-hand panel) for these two samples, with the dashed line corresponding to the fit for the bulk moment and the solid line for the best-fit value. It can be clearly seen that in each case the moment is enhanced from the bulk value. Values of the layer-averaged moment of $2.50\pm0.10\mu_B$ and $2.6\pm0.2\mu_B$ are determined for the Cu/5.7 Fe and Pd/5.7 Fe samples, respectively. A larger error is obtained for the measurements on these samples in comparison with that obtained for the first version samples due to the increased diffuse scattering and poorer surface flatness. The spin asymmetry shown is corrected for diffuse scattering in each case, but this procedure introduces larger errors than for the samples with small solid angle. However within experimental error, the estimates of the absolute value of the magnetic moment are in agreement for the two investigations (see Table II). This provides important confirmation of the enhanced moments in the Cu/Fe and Pd/Fe systems reported previously,[12] and the results demonstrate the reliability of the PNR measurements and estimated accuracy. A greater accuracy is achieved in the present work in comparison with that achieved previously because of the correction for diffuse scattering.

The question of the structures best suited to PNR magnetometry is an important one: for thin overlayers the wave vector at which the spin asymmetry first peaks is large, and hence a background subtraction needs to be carefully made. Also the diffuse scattering needs to be subtracted at a large wave vector, making thicker overlayers desirable from this viewpoint, but the value of the wave vector at which diffuse scattering begins to be significant is sensitively dependent on the roughness spectrum, as we have seen. However, there is clearly an upper limit in the usable overlayer thickness, since the enhancement peak is shifted closer to the critical wave vector with increasing thickness, where beam distortion (due to the incident wave-vector spread and a lack of surface flatness) is important. Our study shows the importance of preparing high-quality samples on sufficiently flat substrates, since the most accurate estimates of the magnetic moment were achieved for samples showing the best flatness but with thinner overlayers.

The combined results obtained for the Ag, Au, Cu, and Pd coated bcc Fe samples are summarized in Table II and Fig. 5, and the result obtained for a Ni/Fe sample prepared by molecular-beam epitaxy using the same methods and investigated previously[11] is also included for completeness. The PNR and FMR measurements of the

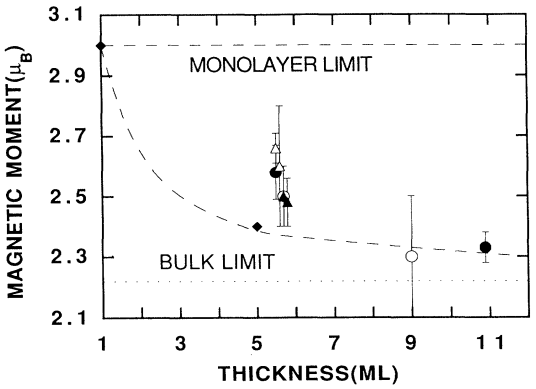

FIG. 5. The values of the layer averaged moment per Fe atom deduced from PNR measurements for samples referred to in Table I and compared with the predictions (Ref. 6) for the layer-averaged moment for 1-ML Fe/Ag(001) and Ag/5-ML Fe/Ag shown as solid diamonds. The dashed line is a guide to the eye only. The Ag/Fe data are shown as solid circles, the Au/Fe data as open circles, the Cu/Fe data as solid triangles, and the Pd/Fe data as open triangles.

magnetization of the samples relative to that of a reference sample are found to agree within experimental error. It is striking that in all cases the Fe moment per atom is found to be significantly enhanced with respect to the bulk value. The Ag/Fe and Au/Fe samples show a reduction in enhancement with increasing thickness, confirming that the enhancement is associated with the interfaces, as predicted by theory.[8,9] These combined results show that the magnetic moment at the Cu/Fe interface is not significantly decreased compared to that at the Ag/Fe interface and the reported decrease of the magnetic moment in Cu/Fe interfaces[10] therefore seems to be incorrect. However, recent x-ray-dichroism measurements have revealed that the Cu can exhibit a small induced moment in Cu/Fe overlayers, which would increase the total moment of the Cu/Fe samples.[36] The result for the Pd/Fe is in reasonable agreement with FMR measurements of the magnetization compared with that of a Au/5.7 Fe reference sample (see Table II), which yield an enhancement of 3 ± 1 % of the Fe/Pd sample magnetization with respect to the Fe/Au sample magnetization. Blugel *et al.*[7] have predicted an induced magnetic moment of $0.32\mu_B$ and $0.17\mu_B$ on the first and second Pd layers, respectively. If this were to occur in our sample then the average magnetic moment per Fe atom deduced from the PNR data would be reduced by approximately $0.1\mu_B$. The accuracy of the combined measurements is therefore insufficient to determine unambiguously whether such an interface polarization occurs or not. However, we can conclude that the Fe layer magnetization is in either case enhanced with respect to the bulk, although we cannot distinguish between the degree of enhancement observed for Fe/Pd and that observed for the other interfaces, with the exception of Cu/Fe. We can certainly exclude the possibility of ferromagnetism occurring in the entire Pd film. It is likely, however, that the increased moment we deduce for the Pd/Fe system is due to a con-

tribution from the interface Pd atoms, and therefore that the moment per Fe atom is very close to that deduced for the Ag/Fe, Au/Fe, and Cu/Fe systems. Making this assumption, to estimate the induced Pd moment we can compare the average moment for the Ag, Au, and Cu coated samples with that of the Pd-coated samples. The measurements on the Ag, Au, and Cu coated Ag(001)/Fe layers of Fe-layer thickness 5.5–5.8 ML reveal an average moment of $2.52\pm0.05\mu_B$. This suggests that for the Pd/5.6 Fe sample the noble-metal interface contributes an additional moment of $0.84\pm0.14\mu_B$ per interface Fe atom (assuming that all the enhancement occurs at the interface) and that the Pd atoms contribute an additional moment per interface Pd atom of $0.78\pm0.39\mu_B$. This value is in very good agreement with recent *ab initio* calculations of the induced moment for a Pd/Fe sandwich structure.[37] For a ferromagnetically coupled 3 Ni/5 Fe/Ag bilayer,[11] the spin asymmetry is consistent with a total moment for the sample, which exceeds that corresponding to the bulk moments, and the Ni moment is estimated to lie in the range $0.5\mu_B-0.8\mu_B$ for the Fe moment in the range $2.5\mu_B-2.7\mu_B$. These results for the average Fe moment are therefore seen to fit well with the thickness-dependent trends observed. No significant differences are found between the degree of enhancement for Ag/Fe and Au/Fe interfaces, in agreement with the theoretical predictions.[8,9] The combined results are compared with the theoretical predictions for the Ag/Fe interface in Fig. 5. It is seen that the experimentally determined values of the moment are, in general, higher than the predicted values for the (5–6)-ML-thick films but that very good agreement is obtained for the 10.9-ML film. The former result is surprising, since in general experimental factors tend to reduce the spin asymmetry (diffuse scattering in particular). It is possible that the trend can be explained by roughness on a scale too small to significantly perturb the neutron reflectivity but large enough to reduce the effective coordination of a significant number of Fe atoms. These experimental results should play a role in stimulating further theoretical work on real interface systems for which roughness is incorporated into the calculations.

V. TEMPERATURE DEPENDENCE OF THE MAGNETIZATION

The temperature-dependent magnetization of ultrathin films is a subject of strong current interest.[38,39] Discussion has focused recently on the role of magnetic anisotropies versus that of dipolar interactions in stabilizing the magnetic order against spin-wave fluctuations. For fcc Co films, recent experimental studies suggest that it is the magnetic anisotropies rather than the dipolar interactions, which stabilize the magnetization.[39,40] The magnetic anisotropy leads to a spin-wave gap T_g from which the temperature-dependent magnetization can be calculated in the spin-wave regime. However, the validity of this model has yet to be widely tested. We therefore studied the temperature-dependent magnetization in selected structures with the same Fe-layer thickness as a test of the spin-wave model. As an input to the calculated behavior, all relevant magnetic anisotropies were determined by FMR, as shown in Table II.

The normalized change in the magnetization of a sample of N_y layers thick as a function of temperature T, in-plane applied field $H_{\rm app}$, and field direction γ is given by:[38]

$$\frac{\Delta M(T,H_{\rm app},\gamma)}{M(0,0,0)}=\frac{T}{N_y T_{\rm ex}}\ln\left[\frac{T}{T_g(H_{\rm app},\gamma)}\right], \quad (12)$$

where $T_{\rm ex}$ is the exchange temperature of the film and $T_g(H_{\rm app},\gamma)$ is the spin-wave gap as a function of applied field and field direction. The gap can be calculated from the energy equation[39]

$$E=K_2\cos^2\theta+K_2'\sin^2\theta\sin^2\phi + \frac{K_4}{4}\sin^4\theta\sin^2 2\phi-MH_{\rm app}\sin\theta\cos(\gamma-\phi), \quad (13)$$

where the magnetization orientation is given by θ the polar angle and ϕ the in-plane azimuthal angle, K_2 is the effective perpendicular uniaxial anisotropy strength (where $K_2/M=2\pi M_{\rm eff}$), K_2' the in-plane uniaxial anisotropy strength, and K_4 the in-plane fourfold anisotropy strength. The gap is then given by[39]

$$T_g(H_{\rm app},\gamma)=\frac{1}{k_B}\left[\left.\frac{\partial^2 E}{\partial\theta^2}\right|_{\theta_0,\phi_0}\left.\frac{\partial^2 E}{\partial\phi^2}\right|_{\theta_0,\phi_0}\right]^{1/2}, \quad (14)$$

and θ_0 and ϕ_0 are the values of θ and ϕ, which minimize E for some value of the applied field and field direction, and are evaluated from

$$\left.\frac{\partial E}{\partial\theta}\right|_{\theta_0,\phi_0}=\left.\frac{\partial E}{\partial\phi}\right|_{\theta_0,\phi_0}=0. \quad (15)$$

The expression for T_g in Eq. (14) can now be used in conjunction with Eq. (12) to calculate the magnetization deviation. Thus the resulting expression for T_g depends on the magnetic anisotropy strengths of the sample and the strength and orientation of the applied field.

In carrying out the measurements, the samples were saturated along the hard [110] axis in plane, and the effect of the applied field was included in calculating the spin-wave gap. In Fig. 6 we show the measured temperature-dependent magnetization for the Ag/5.5 Fe, Au/5.7 Fe, Cu/5.7 Fe, and Pd/5.7 Fe samples. The larger scatter for the Ag/Fe sample, in comparison with the other samples, is due to a smaller counting time per point being used. A reduction in the magnetization in the range 12–20% is observed in the range 4–300 K, with the smallest reduction observed for the Pd/5.7 Fe sample. In each figure the solid line corresponds to a best fit of the form given in Eq. (12) with T_g as the adjustable parameter, and the dashed line corresponds to a fit of the same form with the gap temperature determined from the FMR measurements of the magnetic anisotropies. In obtaining the fits to the PNR data, the spin-wave gap is treated as a variable parameter, and the exchange temperature for bulk Fe (2300 K) is used. The upper and lower bound for the best-fit gap temperature, T_{g1} and T_{g2},

are estimated from a χ^2 analysis and define the estimated range of possible values. The fits are summarized in Table III, where the gap obtained by PNR is compared with that calculated using the anisotropy constants determined by FMR. It can be seen that good agreement is obtained for the Ag/5.5 Fe and Cu/5.7 Fe samples, for which the largest reduction in the magnetization is observed, suggesting that the spin-wave theory is valid in this case. The close agreement reflects the higher-quality data obtained for these two samples. The larger values of the gap obtained from FMR for the Pd/5.7 Fe and Au/5.7 Fe samples are consistent with the weaker temperature dependence of the magnetization observed. However, the values of the gap temperature obtained by FMR lie outside the range estimated from the PNR data. This result may reflect the poorer quality of the data obtained for these two samples and does not necessarily invalidate spin-wave theory. However, it is interesting that the largest gap is obtained for the Pd/Fe sample in both the FMR and PNR experiments, since in this sample the interface magnetism is likely to play the most marked role. Clearly more accurate investigations of the Pd/Fe system are required in future to clarify the role of the Pd interface in influencing the temperature-dependent magnetization. It is interesting in this context to note that FMR studies of exchange coupling in Fe/Pd/Fe(001) epitaxial sandwich structures suggest that the Pd polarization fluctuations are strongly temperature dependent, giving rise to an increase in coupling strength with reduced temperature.[41,42] This may account for the increased effective gap temperature we find for the Pd/Fe system.

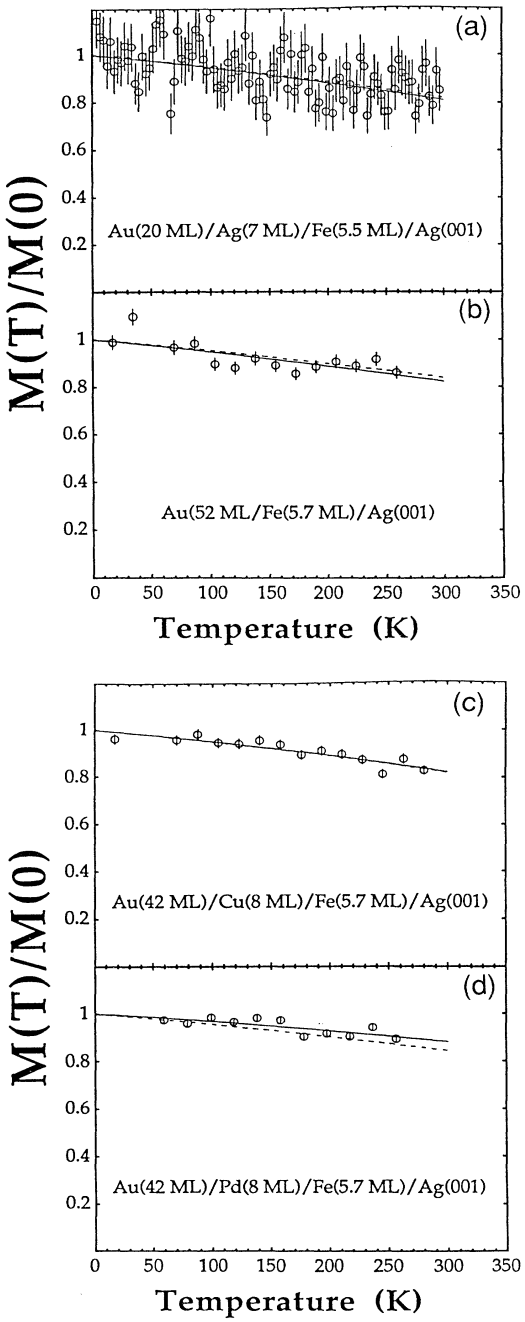

FIG. 6. The temperature-dependent magnetization $M(T)/M(0)$ determined by PNR for (a) the Ag/5.5 Fe, (b) Au/5.7 Fe, (c) Cu/5.7 Fe, and (d) Pd/5.7 Fe samples. In each panel the solid line corresponds to a best fit of the form of Eq. (12) to T_g and the dashed line corresponds to a fit of the form of Eq. (12) with the gap temperature determined from the FMR measurements.

VI. SUMMARY AND CONCLUSION

We have reported the results of a systematic investigation of the magnetic moment per atom in ultrathin Fe/Ag(001) structures using both PNR and FMR techniques, where the Fe films were covered with overlayers of Au, Ag, Cu, and Pd in order to study the effect of the overlayer on the magnetic moment. We find conclusive evidence for strong enhancements of the magnetic moment for each of the Ag/Fe, Au/Fe, Cu/Fe, and Pd/Fe overlayer systems for bcc Fe films prepared on Ag(001) substrates. The enhancement is estimated to lie in the range 12–20 %. Within experimental error, the enhancement for the Pd/Fe system exceeds that of the Cu/Fe system, while the enhancement deduced for the Ag/Fe and Au/Fe systems lies within the range estimated for the Cu/Fe and Pd/Fe systems. In all cases the inclusion of the diffuse scattering correction improves the accuracy of the estimated moment. The correction depends not only on the flatness of the samples but increases with the solid angle over which the reflected intensity is collected. The enhancement is deduced to an estimated accuracy of 4% using a solid angle of 7×10^{-6} sterad. These results resolve the conflicting results of earlier studies and demonstrate the importance of correcting for diffuse scattering in PNR magnetometry.

The temperature dependence of the magnetization has also been measured using PNR, and the results compared with that predicted from spin-wave theory assuming a spin-wave gap calculated from the anisotropy strengths determined from FMR measurements. A reduction in the magnetization of 12–20 % is observed in the range 4–300 K. The strongest temperature dependence is found for the Ag/Fe system, and this is consistent within experimental error with the anisotropy constants determined by FMR. The weakest temperature dependence is

TABLE III. The spin-wave gap temperatures for selected samples deduced from fits to the PNR measurements of the temperature-dependent magnetization. The second and third columns give the range of possible values for the gap temperature, the fourth column gives the value, which best fits the PNR data, and the fifth column gives the spin-wave gap calculated from the anisotropy constants determined by FMR.

Sample (Thicknesses in ML)	T_{g1} (PNR) (K)	T_{g2} (PNR) (K)	T_g (PNR) (K)	T_g (FMR) (K)
20 Au/7 Ag/5.5 Fe/Ag(001)	0.04	0.25	0.10	0.15
52 Au/5.7 Fe/Ag(001)	0.08	0.25	0.14	0.29
42 Au/8 Cu/5.7 Fe/Ag (001)	0.07	0.21	0.12	0.11
42 Au/8 Pd/5.7 Fe/Ag(001)	1.20	2.50	1.76	0.34

found for the Pd/Fe system, and here the value of the spin-wave gap determined by FMR is smaller than the value obtained from fitting the PNR data. The gap is found to lie in the kelvin range, although the temperature dependence is found to be relatively insensitive to the magnitude of the gap.

ACKNOWLEDGMENTS

We would like to thank the SERC for financial support and ILL, Grenoble for the provision of experimental facilities for the PNR studies.

*Present address: Optical Science Center, University of Arizona, Tucson, Arizona 85721.

[1]C. L. Fu, A. J. Freeman, and T. Oguchi, Phys. Rev. Lett. **54**, 2700 (1985).

[2]J. Korecki and U. Gradmann, Phys. Rev. Lett. **55**, 2491 (1985).

[3]U. Gradmann, M. Przyblyski, H. J. Elmers, and G. Liu, Appl. Phys. A **49**, 563 (1989).

[4]D. A. Newstead, C. Norris, C. Binns, and P. C. Stephenson, J. Phys. C **20**, 6245 (1987).

[5]U. Gradmann and M. Przyblyski, in *Thin Film Growth for Low Dimensional Structures,* edited by R. F. C. Farrow, S. S. P. Parkin, P. J. Dobson, J. H. Neave, and A. S. Arrott (Plenum, New York, 1987).

[6]S. Ohnishi, M. Weinert, and A. J. Freeman, Phys. Rev. B **30**, 36 (1984).

[7]S. Blugel, B. Drittler, R. Zeller, and P. H. Dederichs, Appl. Phys. A **49**, 547 (1989).

[8]S. Ohnishi, M. Weinert, and A. J. Freeman, Phys. Rev. B **30**, 36 (1984).

[9]M. E. McHenry, J. M. Maclaren, M. E. Eberhart, and S. Crampin, J. Magn. Magn. Mater. **88**, 134 (1990).

[10]C. L. Fu and A. J. Freeman, Phys. Rev. B **35**, 925 (1987).

[11]J. A. C. Bland, R. D. Bateson, A. D. Johnson, B. Heinrich, Z. Celinski, and H. J. Lauter, J. Magn. Magn. Mater. **93**, 331 (1991).

[12]J. A. C. Bland, R. D. Bateson, B. Heinrich, Z. Celinski, and H. J. Lauter, J. Magn. Magn. Mater. **104-107**, 1909 (1992).

[13]R. D. Bateson, G. W. Ford, J. A. C. Bland, H. J. Lauter, B. Heinrich, Z. Celinski, and H. J. Lauter, J. Magn. Magn. Mater. **121**, 189 (1993).

[14]B. Heinrich, Z. Celinski, J. F. Cochran, A. S. Arrott, and K. Myrtle, J. Appl. Phys. **70**, 5769 (1991).

[15]J. A. C. Bland, in *Ultrathin Magnetic Structures, Vol. 1,* edited by J. A. C. Bland and B. Heinrich (Springer-Verlag, Berlin, 1994).

[16]J. A. C. Bland, A. D. Johnson, C. Norris, and H. J. Lauter, J. Appl. Phys. **67**, 5397 (1990).

[17]B. Heinrich, in *Ultrathin Magnetic Structures, Vol. 2,* edited by B. Heinrich and J. A. C. Bland (Springer-Verlag, Berlin, 1994).

[18]B. Heinrich, S. T. Purcell, J. R. Dutcher, K. B. Urquhart, J. F. Cochran, and A. S. Arrott, Phys. Rev. B **38**, 12 879 (1988).

[19]B. Heinrich, Z. Celinski, J. F. Cochran, W. B. Muir, J. Rudd, Q. M. Zhong, A. S. Arrott, K. Myrtle, and J. Kirschner, Phys. Rev. Lett. **64**, 673 (1990).

[20]B. Heinrich, Z. Celinski, J. F. Cochran, A. S. Arrott, and K. Myrtle, Phys. Rev. B **47**, 5077 (1993).

[21]Z. Celinski, B. Heinrich, J. F. Cochran, W. B. Muir, A. S. Arrott, and J. Kirschner, Phys. Rev. Lett. **65**, 1156 (1990).

[22]H. Chen, N. E. Brener, and J. Callaway, Phys. Rev. B **40**, 1443 (1990).

[23]E. E. Fullerton, B. Heinrich, and Z. Celinski (unpublished).

[24]W. F. Egelhoff, Jr., Mater. Res. Symp. Proc. **229**, 27 (1991).

[25]G. P. Felcher, R. O. Hilleke, R. K. Crawford, J. Haumann, R. Kleb, and G. Ostrowski, Rev. Sci. Instrum. **58**, 609 (1987); S. J. Blundell and J. A. C. Bland, Phys. Rev. B **46**, 3391 (1992).

[26]S. J. Blundell and J. A. C. Bland, J. Magn. Magn. Mater. **121**, 185 (1993).

[27]Y. Y. Huang, C. Liu, and G. P. Felcher, Phys. Rev. B **47**, 183 (1993).

[28]L. Nevot and P. Croce, Rev. Phys. Appl. **15**, 761 (1980).

[29]J. A. de Santo and R. J. Wombell, *Waves Random Media* **1**, S41 (1991).

[30]S. K. Sinha, E. B. Sirota, S. Garoff, and H. B. Stanley, Phys. Rev. B **38**, 2297 (1988).

[31]A. Steyerl, Z. Phys. **254**, 169 (1972).

[32]The solid angle is incorrectly given as 2.8×10^{-4} sterad in Ref. 13.

[33]Z. Celinski, B. Heinrich, and J. F. Cochran, J. Appl. Phys. **73**, 5966 (1993).

[34]P. J. Schurer, Z. Celinski, and B. Heinrich, Phys. Rev. B **48**, 2577 (1993).

[35]J. A. C. Bland, A. D. Johnson, R. D. Bateson, S. J. Blundell, H. J. Lauter, C. Shackleton, and J. Penfold, J. Magn. Magn. Mater. **93**, 513 (1991).

[36]C. Schneider (private communication).

[37]E. E. Fullerton, B. Heinrich, Z. Celinski, J. A. C. Bland, K. Ounadjela, and D. Stoeffler (unpublished).

[38]P. Bruno, Phys. Rev. B **43**, 6015 (1991).
[39]J. A. C. Bland, G. A. Gehring, B. Kaplan, and C. Daboo, J. Magn. Magn. Mater. **113**, 173 (1992).
[40]P. Krams, F. Lauks, R. L. Stamps, B. Hillebrands, and G. Guntherodt, Phys. Rev. Lett. **69**, 3674 (1992).
[41]B. Heinrich, Z. Celinski, and K. Myrtle, J. F. Cochran, A. S. Arrot, and J. Kirschner, J. Magn. Magn. Mater. **93**, 75 (1991).
[42]Z. Celinski, B. Heinrich, and J. Cochran, J. Appl. Phys. **70**, 5870 (1991).